Energy Engineering
DOI: 10.32604/EE.2020.010433
Article

Experimental Study on Flow and Heat Transfer Characteristics of Nanofluids in a Triangular Tube at Different Rotation Angles

Cong Qi[1,2,*], Chengchao Wang[1,2], Jinghua Tang[1,2] and Dongtai Han[2]

[1]Jiangsu Province Engineering Laboratory of High Efficient Energy Storage Technology and Equipments, China University of Mining and Technology, Xuzhou, 221116, China

[2]School of Electrical and Power Engineering, China University of Mining and Technology, Xuzhou, 221116, China

[*]Corresponding Author: Cong Qi. Email: qicong@cumt.edu.cn

Received: 04 March 2020; Accepted: 14 April 2020

Abstract: Because of the poor thermal performance of ordinary tubes, a triangular tube was used to replace the smooth channel in the heat transfer system, and nanofluids were used to take the place of ordinary fluids as the heat transfer medium. High stability nanofluids were prepared, and an experimental set on flow and heat exchange was established. Effects of triangular tube rotation angles (α = 0°, 30°, 60°) as well as mass fractions of nanofluids (ω = 0.1%, 0.3%, 0.5%) on heat exchange and flow performance were experimentally considered at Reynolds numbers (Re = 800–8000). It was shown that the triangular tube with a rotation angle α = 0° possesses the most excellent thermal property, followed by a rotation angle α = 60° triangular tube, and a rotation angle α = 30° triangular tube has the worst heat exchange property. Results also revealed that resistance coefficients of the triangular tube with rotation angles α = 0° and α = 30° are close to each other, and a rotation angle α = 60° triangular tube shows the minimal resistance coefficient. It could be also seen that higher nanoparticle mass fraction can augment the thermal performance. However, higher nanoparticle mass fraction can also lead to an increment in resistance coefficient. A comprehensive performance evaluation index was introduced to appraise the augment in Nusselt number and flow resistance coefficient. The experiment revealed that the highest index emerges with nanofluids (ω = 0.5%) in the triangular tube with a rotation angle α = 0°.

Keywords: Nanofluids; forced convection; heat transfer enhancement; triangular tube; rotation angle

Nomenclature

A_c	sectional area of triangle tube, m^2
c_p	specific heat capacity of nanofluids, $J \cdot kg^{-1} \cdot K^{-1}$
c_{pb}	specific heat capacity of base fluid, $J \cdot kg^{-1} \cdot K^{-1}$
c_{pp}	specific heat capacity of nanoparticle, $J \cdot kg^{-1} \cdot K^{-1}$
d_e	hydraulic diameter, m
f	flow resistance coefficient of nanofluids
h	convective heat transfer coefficient, $W \cdot m^{-2} \cdot K^{-1}$
L	length of triangle tube, m
Nu	Nusselt number of nanofluids
P'	wetted perimeter, m
p	pressure drop, Pa
$\Delta P/\Delta l$	pressure drop per unit length, $Pa \cdot m^{-1}$
q_m	mass flow rate, kg/s

Q_j heating power, W
Q_r heat absorption of nanofluids, W
Re Reynolds number
r_i inner radius, m
r_o outer radius, m
T_{in} inlet temperatures, K
T_{out} outlet temperatures, K
T_{wi} temperature of the inner wall, K
T_{wo} temperature of the outer wall, K
T_f average temperature of nanofluids, K
u velocity of fluid, m/s

Greek symbols

α rotation angle, °
ρ density of nanofluids, $kg \cdot m^{-3}$
ρ_b density of base fluid, $kg \cdot m^{-3}$
ρ_p density of nanoparticle, $kg \cdot m^{-3}$
ω nanoparticle mass fraction, %
λ thermal conductivity of tube, $W \cdot m^{-1} \cdot K^{-1}$
λ_f thermal conductivity of nanofluids, $W \cdot m^{-1} \cdot K^{-1}$
μ_f dynamic viscosity of nanofluids, Pa·s
ξ comprehensive performance index

Subscripts

b base fluid
f nanofluids
in inlet
out outlet
p nanoparticle
w the wall of tube

1 Introduction

In the field of industry, the power of heat exchange equipment is increasing. However, due to the low thermal conductivity heat-transfer media (air, water) and the inefficient thermal performance of smooth tube, enhanced heat transfer technology is urgently needed.

Nanofluids show extraordinary thermal performance. Esfe et al. [1] indicated that the thermophysical parameters of SWCNTs-MgO/EG hybrid nanofluids augment with the volume fraction. Akhgar et al. [2] predicted the thermophysical parameters of MWCNT-TiO_2/water-ethylene glycol hybrid nanofluids by ANNS. Wang et al. [3] also predicted the thermal conductivity of nanofluids by artificial neural network. Hence, they are used in a multitude of heat exchange applications, such as solar thermal conversion [4,5], boiling heat exchange [6,7], and so forth. Li et al. [8] discussed the free convection of magnetic nanofluids in sinusoidal annulus. Izadi et al. [9] discussed the laminar flow of nanofluids in the two eccentric cylinders and a C-shaped cavity [10] respectively. Zhao et al. [11] investigated the CPU cooled by nanofluids and rectangular grooves, and found that the temperature of CPU is reduced by 12.5%.

Many researchers have conducted many studies in compulsive convection. Sheikholeslami et al. discussed the compulsive convection of nanofluids in a lid drive 3D enclosure [12] and a solar system [13] respectively. Results indicated that high lid velocity, permeability and revolution cause an increase in Nu, but the high Lorentz force reduces it. Karimipour et al. studied the forced convection of water, carbon nanotubes-water nanofluids [14] and copper-water nanofluids [15] in a microchannel respectively. They discovered that the magnetic field is beneficial to the heat flux at the thermally developing region, and the

wall slip velocity is also a favorable factor for the heat exchange. Sun et al. analyzed the heat exchange of nanofluids in a channel under magnetic field [16] and also studied the convection impinging jets [17]. It was indicated that the magnetic field has a beneficial effect on the thermal property, and the swirling impinging jets has more superiority than common impinging jets. Mei et al. discussed the forced convection of nanofluids in a circular tube under horizontal magnetic field [18]. Results showed that the enhanced tubes can contribute to the thermal performance, but the paralleled magnetic field has a negative effect.

From above references, the enhanced technologies and nanofluids not only promote the thermal performance but also magnify the flow resistance. Hence, it is necessary to develop a comprehensive assessment method. Some investigators used comprehensive assessment methods to analyze these, such as entropy generation [19]. In addition, compared to the smooth tube, the triangular tube has a smaller hydraulic diameter under the same sectional area, which can increase the disturbance in the channel to enhance the heat exchange. Besides, considering the stable structure of triangle, triangular tube can be applied in various fields. Hence, the target of the article is to systematically research the turbulent flow of nanofluids in a triangular tube at diverse rotation angles. Since the triangle is not completely symmetrical structure, different angles may affect the flow resistance and heat transfer. Different parameters, such as triangular tube rotation angles (α = 0°, 30°, 60°), mass fractions of nanoparticle (ω = 0.1%, 0.3%, 0.5%) and Reynolds numbers (Re = 800–8000), are considered to explore the mechanisms of the heat and flow performance. Also, a comprehensive performance evaluation index is introduced to appraise the thermal-hydraulic performance of nanofluids in enhanced tubes, which can contribute to the design and operation of heat-exchange equipment. The innovations of this paper are as below: (1) Triangular tubes with different rotation angles are considered to explore the mechanisms of the heat and flow performance. (2) The comprehensive performance is studied by a comprehensive evaluation performance index.

2 Methods

2.1 Nanofluids

In this paper, TiO_2-water nanofluids are adopted as the working medium, since the high sterilization, stability and excellent thermal conductivity of TiO_2 nanoparticles. The diameter of the TiO_2 nanoparticle is around 10 nm, because the nanofluids with nanoparticles of this size have high stability and thermal conductivity, which can reduce the deposition and agglomeration in tube and enhance the heat exchange. The working medium is produced by a two-step method. Firstly, a proper dose of dispersant agent is mixed into the pure water to ensure the stability of nanofluids. After being stirred for some time, TiO_2 nanoparticles with certain mass fractions are added. Then some NaOH is added to regulate the pH value and fluid continues to be stirred. At last the ultrasonic vibration is used to prepare the nanofluids. The prepared TiO_2-H_2O nanofluids with three mass fractions of nanoparticle (ω = 0.1%, 0.3%, 0.5%) are shown in Fig. 1. In this paper, precipitation method is introduced to examine the stability of TiO_2-H_2O nanofluids, results demonstrate that TiO_2-H_2O nanofluids still remain well stability after standing seven days, thus illustrating the nanofluids prepared have well stability.

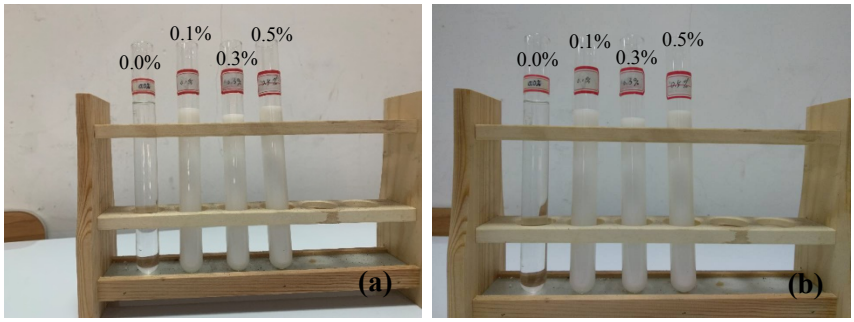

Figure 1: Nanofluids prepared by two-step method, (a) before standing, (b) after standing for 7 days

2.2 Experimental System

An experimental set for nanofluids forced convection is established, which is shown in Fig. 2. The core section is the triangular tube which is presented in Fig. 3. For the purpose of preventing the entrance effect, a length of 100 mm at two ends of tube is left respectively. A DC power connected to a heating wire supplies the heat for the triangular tube, and the application of eleven thermocouples is adopted to

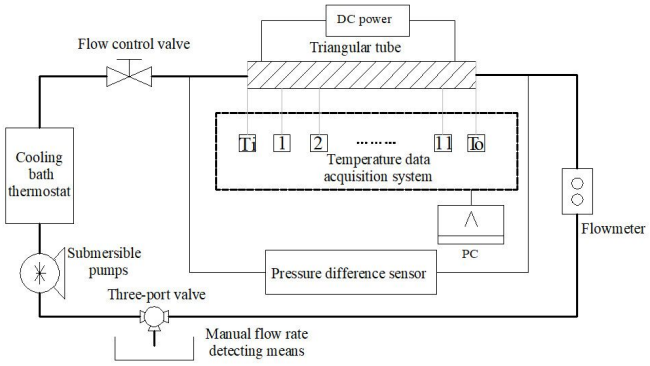

Figure 2: Schematic diagram of experimental system

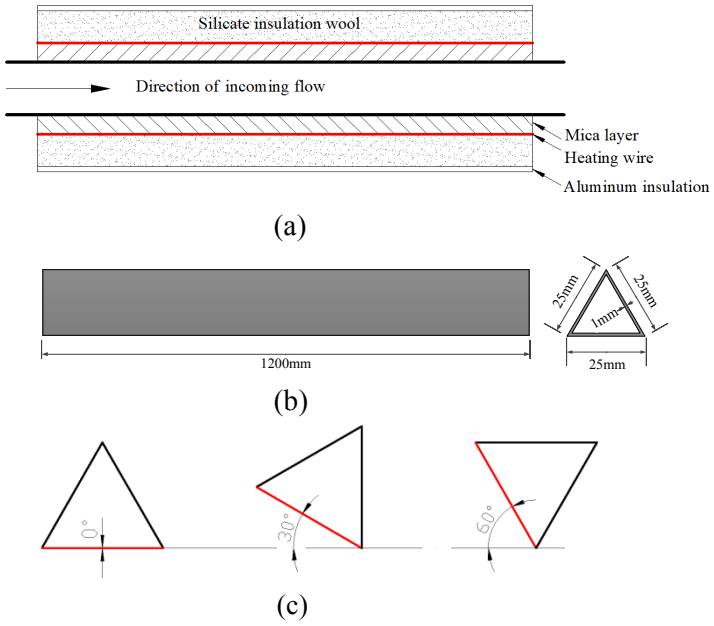

Figure 3: Triangle tube, (a) internal diagram, (b) size dimension, (c) rotation angle

record the outside wall temperature of the triangular tube, besides, the pressure drop is measured by a pressure difference sensor. The cooling bath thermostat is adopted to control the temperature of the nanofluids. To maintain the insulation and prevent the heat dissipation, mica layer, silicate insulation wool and aluminum insulation are adopted, and the details can be seen from Fig. 3(a). The size of the triangular tube is presented in Fig. 3(b). Three rotation angles (α = 0°, 30°, 60°) are adopted in this experiment, and the details can be seen from Fig. 3(c).

2.3 Data Processing

The hydraulic diameter of the triangle tube can be computed as below:

$$d_e = \frac{4A_c}{P'} \tag{1}$$

Reynolds number is:

$$Re = \frac{\rho u d_e}{\mu_f} \tag{2}$$

DC power heating power is:

$$Q_j = UI \tag{3}$$

Heat absorption of the fluid is:

$$Q_r = c_p q_m (T_{out} - T_{in}) \tag{4}$$

Convective heat transfer coefficient is:

$$h_f = \frac{Q_r}{\pi d_e L\left(T_{wi} - T_f\right)} \tag{5}$$

Average temperature of the external wall of the triangle tube can be computed:

$$T_{wo} = \frac{\sum_{i=1}^{11} T_{wo}(i)}{11} \tag{6}$$

Average temperature of the internal wall of the triangle tube can be computed:

$$T_{wi} = T_{wo} - \frac{Q_f \, ln\left(r_o / r_i\right)}{2\pi\lambda l} \tag{7}$$

Average temperature of the fluid is presented as below:

$$T_f = \frac{T_{in} + T_{out}}{2} \tag{8}$$

Nusselt number can be defined as follows:

$$Nu = \frac{h_f d_e}{\lambda_f} \tag{9}$$

Resistance coefficient is:

$$f = \frac{2d_e}{\rho u^3} \cdot \frac{\Delta p}{\Delta l} \tag{10}$$

Specific heat and density are presented as below respectively [20]:

$$c_p = \left(1 - \varphi\right) c_{pb} + \varphi c_{pp} \tag{11}$$

$$\rho = \left(1 - \varphi\right) \rho_b + \varphi \rho_p \tag{12}$$

Comprehensive performance index for flow and heat exchange is [21]:

$$\xi = \left(\frac{Nu}{Nu_{bf}}\right) \Big/ \left(\frac{f}{f_{bf}}\right)^{\frac{1}{3}} \tag{13}$$

2.4 Uncertainty Analysis

For the purpose of guaranteeing the reliability of the experimental system, uncertainty analysis is essential. The uncertainties of thermal-hydraulic performances (*Nu* and *f*) are defined as follows [21]:

$$\frac{\delta Nu}{Nu} = \sqrt{(\frac{\delta Q_r}{Q_r})^2 + (\frac{\delta T}{T})^2} \tag{14}$$

$$\frac{\delta f}{f} = \sqrt{(\frac{\delta q_m}{q_m})^2 + (\frac{\delta L}{L})^2 + (\frac{\delta p}{p})^2} \tag{15}$$

Based on Eqs. (14) and (15), the uncertainties of thermal-hydraulic performances (*Nu* and *f*) are obtained which can be seen in Tab. 1. All the data of temperature and pressure drop are recorded about 60 minutes until stable to guarantee the precision of the experiment.

Table 1: Uncertainty of the experiment

Physical quantity	DC power	Temperature	*Nu*	Pressure drop	Tube length	Mass Flow	*f*
Uncertainty	±1.0%	±1.0%	±1.4%	±0.5%	±0.1%	±1.1%	±1.1%

3 Results and Discussion

3.1 Experimental Verification

The experimental verification, which is prior to the formal experiment, is carried out. The experiment results of this paper are compared with those of other references [22,23] and those calculated by Eq. (16) in Fig. 4. The figure illustrates good agreement between the results, whose max errors are less than 6.6% and 1.4% for Nusselt number and flow resistance coefficient respectively, thus demonstrating that the experiment system has well reliability.

The Filonenko formula [24]:

$$f = (1.82 \lg Re - 1.64)^{-2} \tag{16}$$

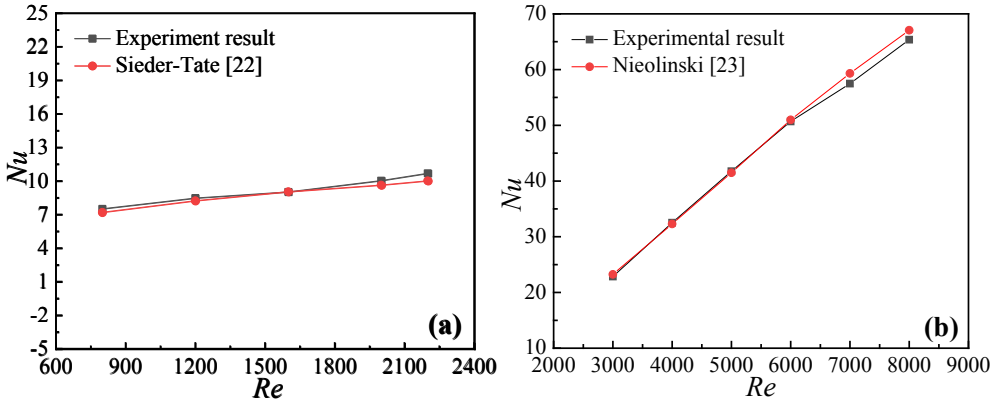

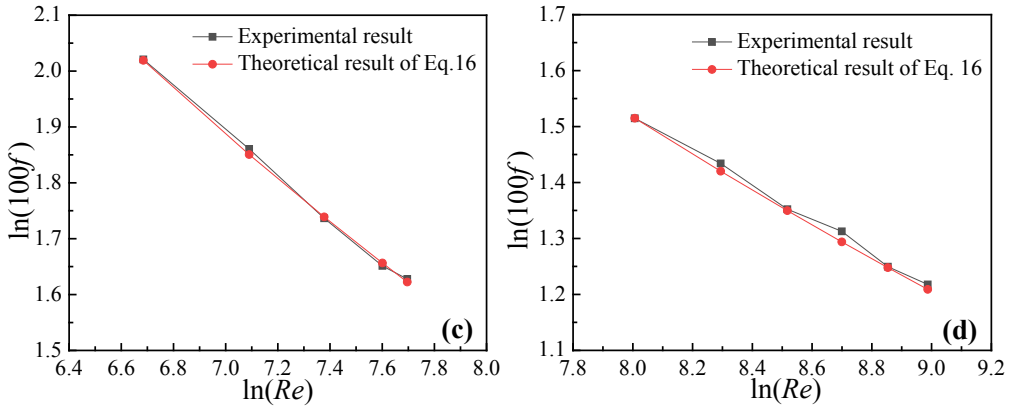

Figure 4: Experimental verification, heat transfer characteristics: (a) laminar flow, (b) turbulent flow; flow characteristics: (c) laminar flow, (d) turbulent flow

3.2 Effects of Rotation Angles

Nusselt numbers of the triangular tubes with rotation angles (α = 0°, 30°, 60°) for laminar and turbulent conditions are investigated in Figs. 5 and 6 respectively. Results indicate that the triangular tube with a rotation angle α = 0° shows the maximal Nusselt number, followed by the triangular tube with a rotation angle α = 60°, and the minimum one is the triangular tube with a rotation angle α = 30°. A comparison between the triangular tubes with rotation angles α = 0° and 30° illustrates that the maximum ratios on enhancing heat transfer are 6.2% and 5.3% for laminar and turbulent conditions respectively. It may be because the triangular tube with a rotation angle α = 0° has the greatest impact on the reduction in laminar boundary layer, and the rotation angle α = 30° shows the minimal influence. A bigger enhancement ratio in Nusselt number for laminar condition is obtained compared to the turbulent condition, due to reasons that the rotation angle has a significant impact on enhancing the heat exchange for laminar condition, however, the effect of the rotation angle can be weakened by the disturbance for turbulent condition, and when the flow state changes from laminar flow to turbulent flow, the enhancement ratio reduces.

The flow resistances of different rotation angles for laminar and turbulent conditions are researched in Figs. 7 and 8 respectively. It is obtained that the resistance coefficients of the triangular tube are close to each other, especially the rotation angles α = 0° and 30°, and the triangular tube with a rotation angle α = 60° behaves the minimal resistance coefficient. In addition, compared with a rotation angle α = 60°, the maximal increments of resistance coefficients are 4.1% and 3.2% in the triangular tube with a rotation angle 30° for laminar and turbulent conditions respectively. This demonstrates that the resistance coefficients relate to the rotation angles directly as well.

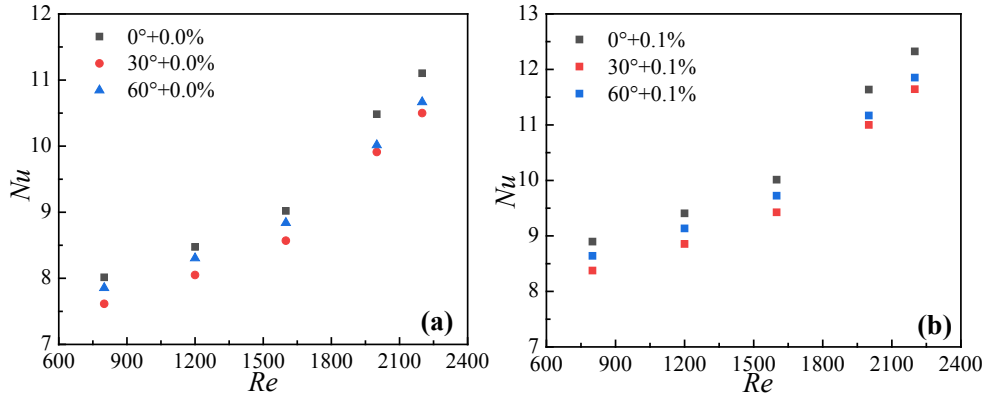

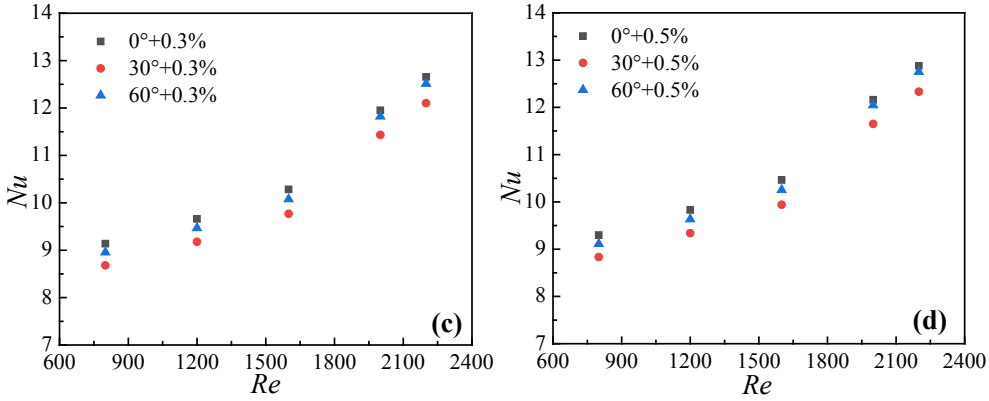

Figure 5: Effects of different rotation angles on Nusselt numbers at laminar flow, (a) 0.0%, (b) 0.1%, (c) 0.3%, (d) 0.5%

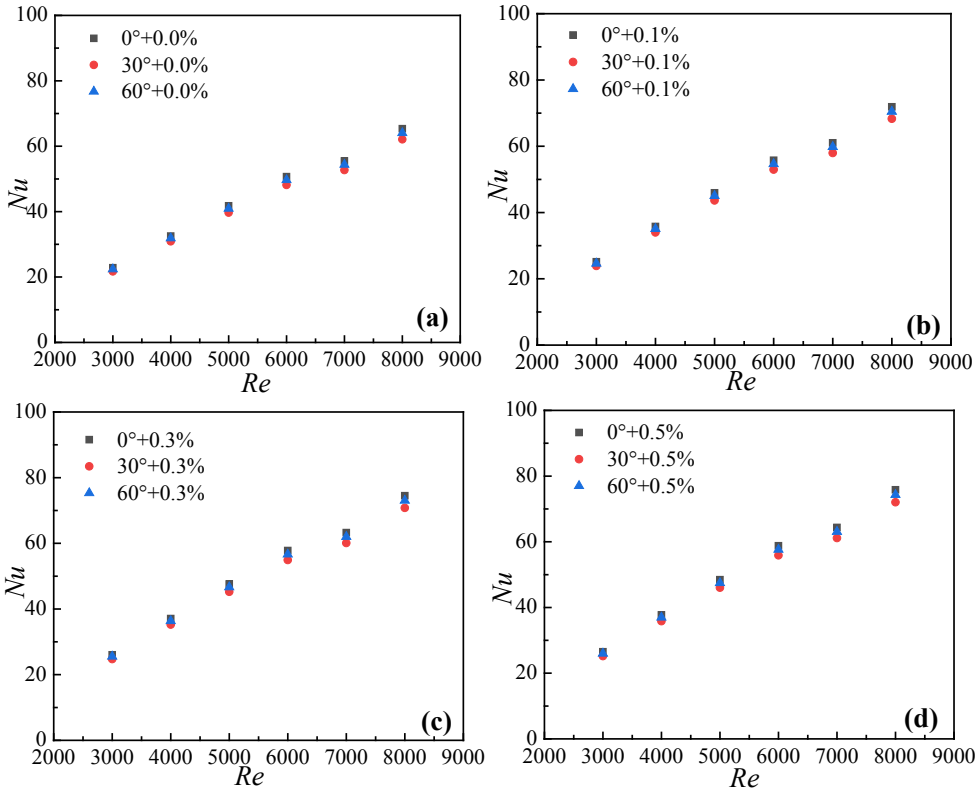

Figure 6: Effects of different rotation angles on Nusselt numbers at turbulent flow, (a) 0.0%, (b) 0.1%, (c) 0.3%, (d) 0.5%

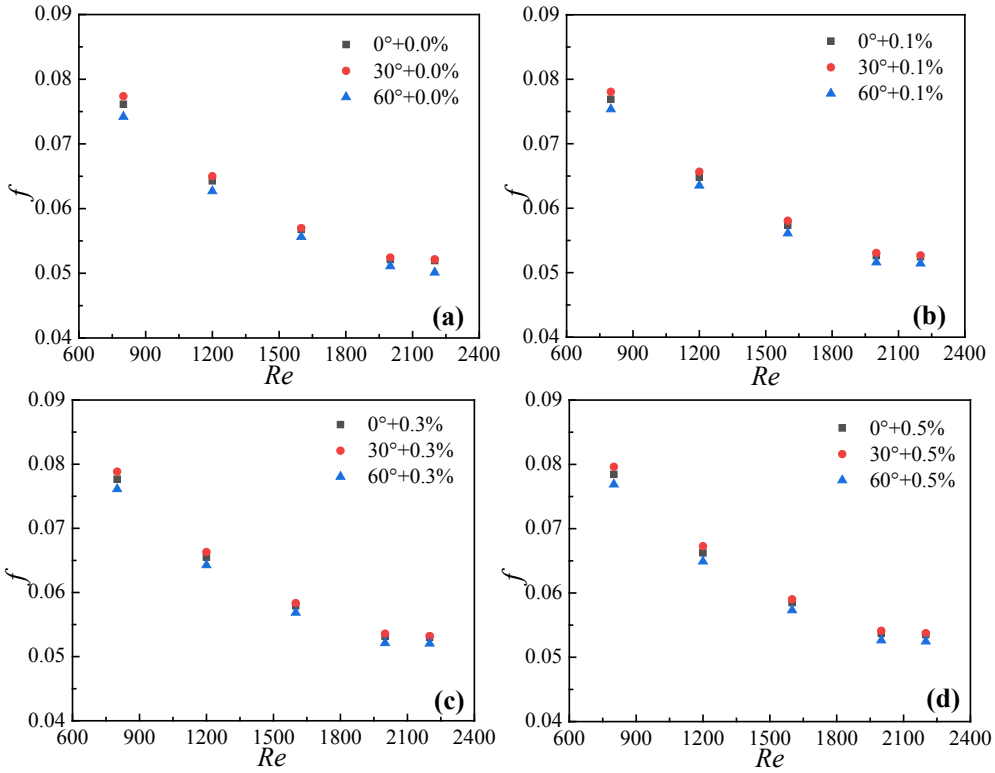

Figure 7: Effects of different rotation angles on the flow resistance at laminar flow, (a) 0.0%, (b) 0.1%, (c) 0.3%, (d) 0.5%

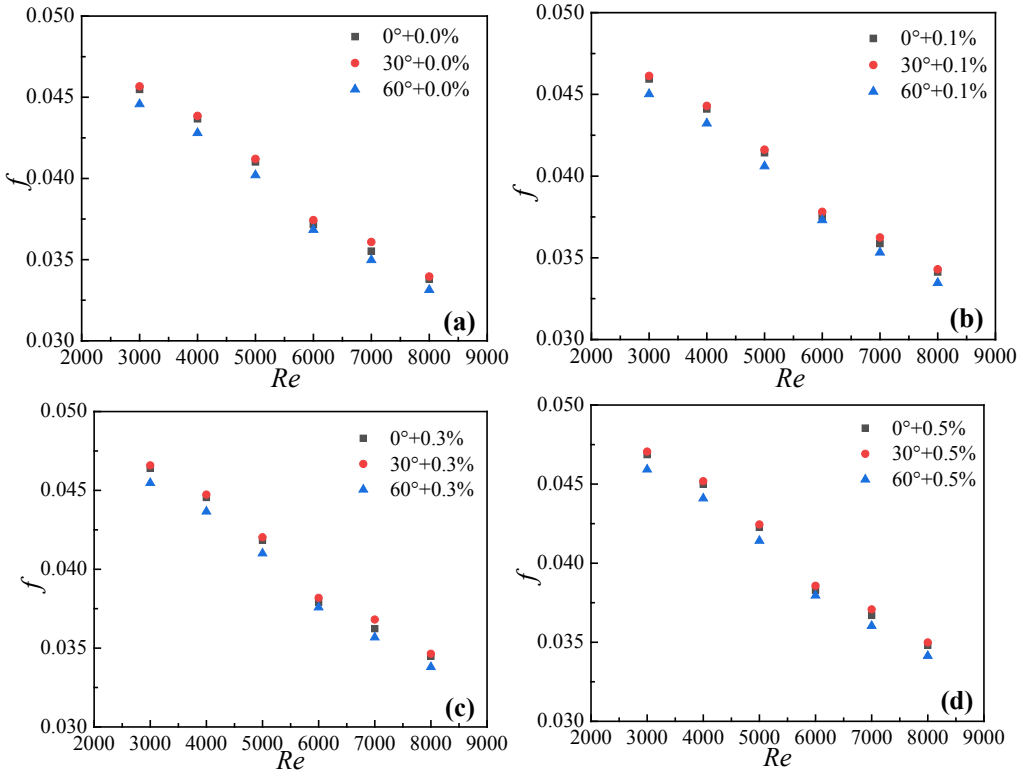

Figure 8: Effects of different rotation angles on the flow resistance at turbulent flow, (a) 0.0%, (b) 0.1%, (c) 0.3%, (d) 0.5%

3.3 Effects of Nanoparticle Mass Fractions

In addition to the different rotation angles, Figs. 9 and 10 give the impacts of mass fractions on Nusselt numbers and resistance coefficients. Results of Fig. 9 explain that Nusselt number and the nanoparticle mass fraction are positively related. A comparison between nanofluids (ω = 0.5%) and pure water illustrates that the growths of the Nusselt number are 20.3% and 16% for laminar and turbulent conditions respectively. The whole thermal conductivity of fluid can be increased with TiO_2 nanoparticles whose thermal conductivity is higher. Besides, nanoscale nanoparticles have the greatest Brownian force compared with other interaction forces [25], which can augment the heat exchange. Besides, a bigger enhancement ratio for the laminar condition is present, compared to the turbulent condition. This reason is similar to Figs. 5 and 6. In laminar regime, the influence of nanoparticle has a positive role in the enhancement ratio, however, the disturbance reduces the impact of nanoparticle in turbulent regime.

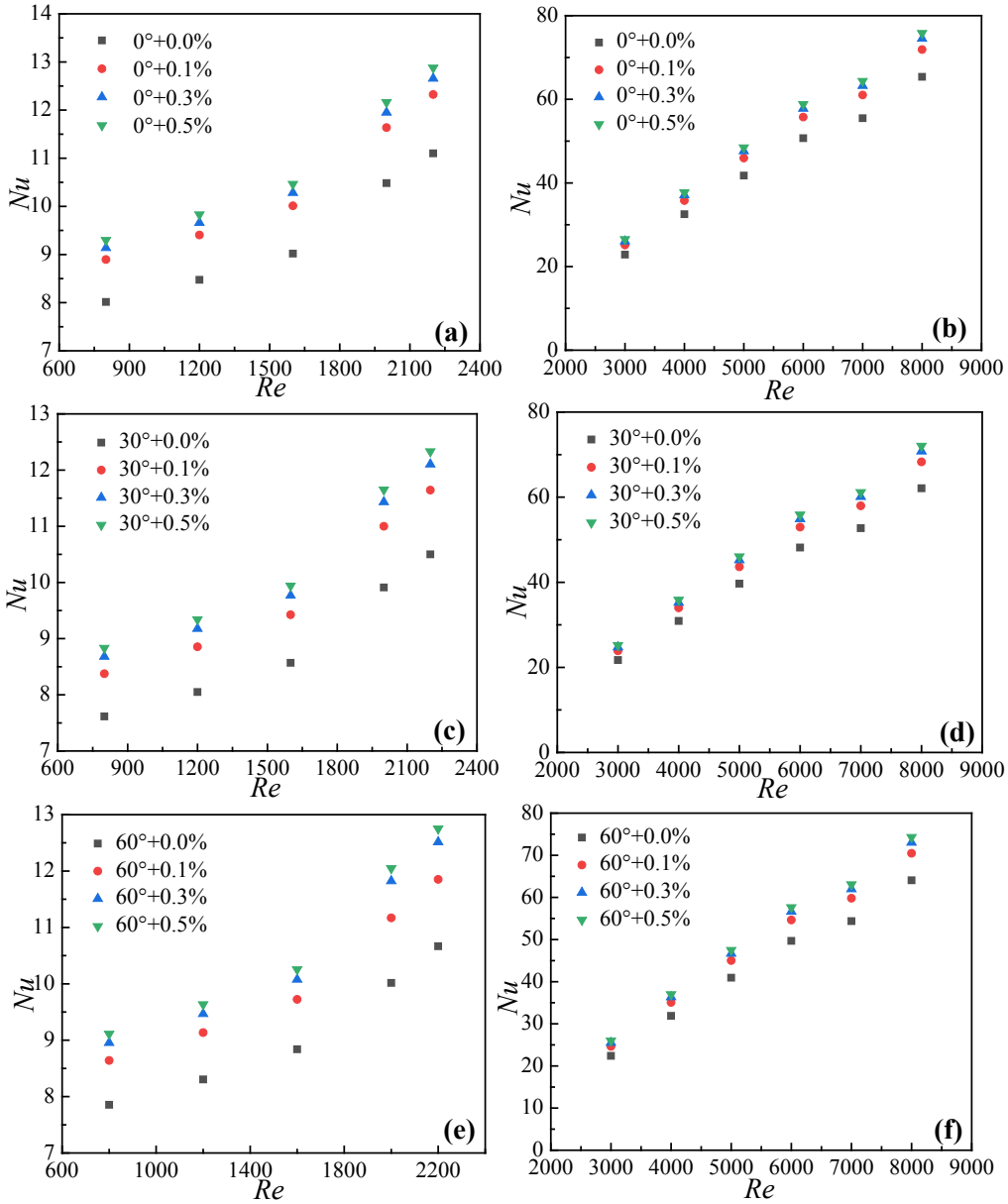

Figure 9: Effects of nanoparticle mass fractions on Nusselt numbers, α = 0°: (a) laminar flow, (b) turbulent flow; α = 30°: (c) laminar flow, (d) turbulent flow; α = 60°: (e) laminar flow, (f) turbulent flow

Changes of flow resistances with nanoparticle mass fractions are researched in Fig. 10. It can be seen that the addition of nanoparticles increases the resistance coefficient. A comparison between nanofluids (ω = 0.5%) and pure water illustrates that the growths of the resistance coefficient are 4.7% and 3.3% for laminar and turbulent conditions respectively. The drag force between water molecules and nanoparticles is caused by the mass differences between them [25], and the drag force is an unbeneficial factor and can increase the viscosity, lastly reduces the heat transfer. Hence, with the increase of nanoparticles, the resistance coefficient shows an increase trend. Results also present that the enhancement in laminar regime is prior to that in turbulent regime, due to reasons that the drag force plays a great role in resistance coefficient in laminar regime, however, the disturbance begins to dominate the flow resistance in turbulent regime.

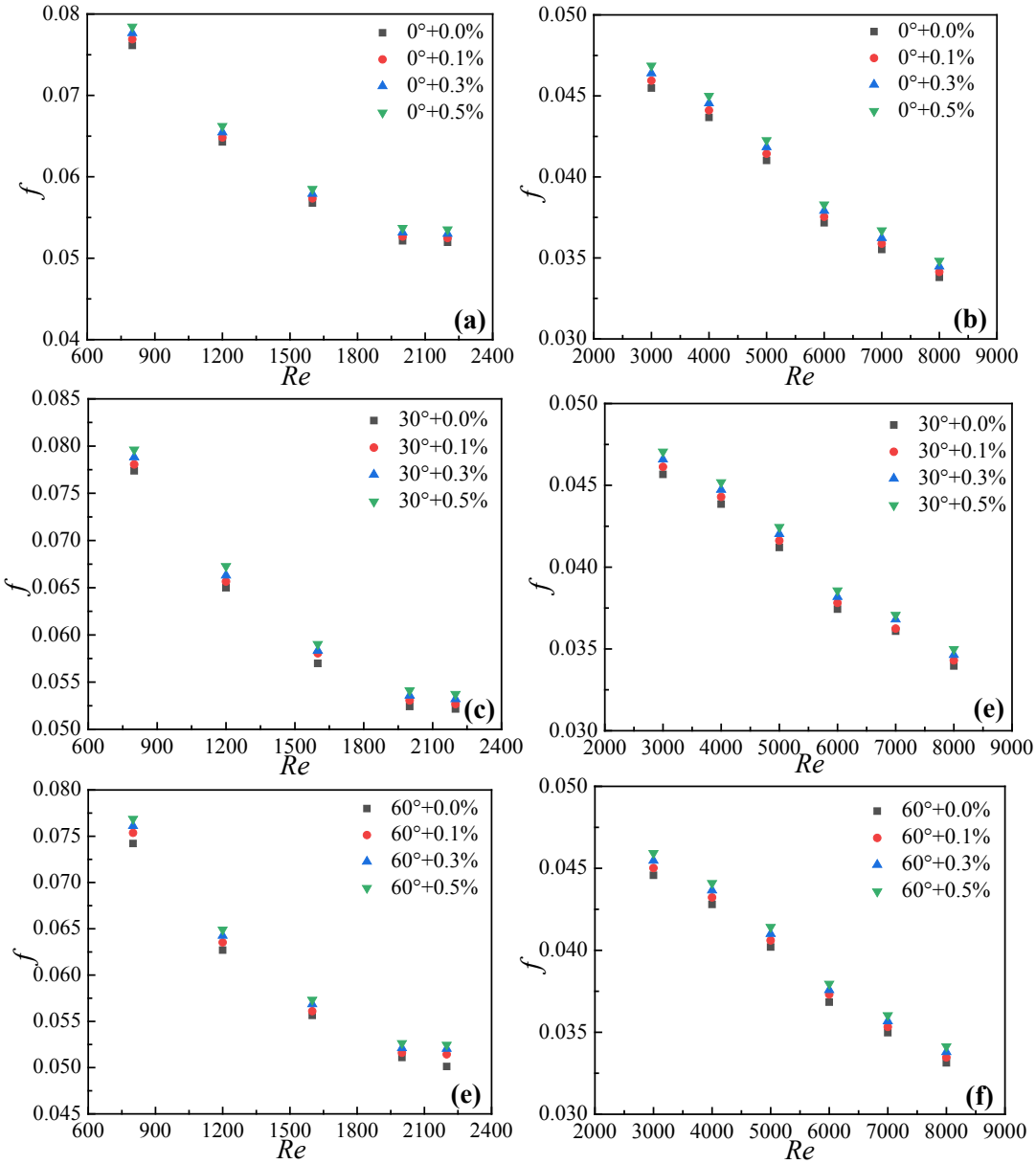

Figure 10: Effects of nanoparticle mass fractions on flow resistance, α = 0°: (a) laminar flow, (b) turbulent flow; α = 30°: (c) laminar flow, (d) turbulent flow; α = 60°: (e) laminar flow, (f) turbulent flow

In order to clearly compare these data, Tabs. 2 and 3 present the Nusselt numbers in laminar and turbulent conditions respectively. Tabs. 4 and 5 show the resistance coefficients in laminar and turbulent conditions respectively.

Table 2: Nusselt numbers in laminar condition

Re	α	ω = 0%	ω = 0.1%	ω = 0.3%	ω = 0.5%
800	0	8.0152	8.89687	9.13732	9.29763
	30	7.61444	8.37588	8.68046	8.83274
	60	7.85489	8.64038	8.95458	9.11167
1200	0	8.47403	9.40617	9.66039	9.82987
	30	8.05033	8.85536	9.17737	9.33838
	60	8.30455	9.13500	9.46718	9.63328
1600	0	9.01995	10.01215	10.28274	10.46314
	30	8.56895	9.42585	9.76861	9.93999
	60	8.30455	9.72351	10.07709	10.25388
2000	0	10.48324	11.6364	11.9509	12.16056
	30	9.91158	10.99954	11.4322	11.64943
	60	10.01579	11.16899	11.82322	12.04731
2200	0	11.10222	12.32347	12.65653	12.87858
	30	10.49961	11.64367	12.10256	12.33155
	60	10.66677	11.85136	12.51474	12.75097

Table 3: Nusselt numbers in turbulent condition

Re	α	ω = 0%	ω = 0.1%	ω = 0.3%	ω = 0.5%
3000	0	22.85134	25.13588	26.05053	26.50756
	30	21.70878	23.87908	24.748	25.18218
	60	22.39432	24.63316	25.52952	25.97741
4000	0	32.52524	35.78177	37.07977	37.72928
	30	30.89898	33.99268	35.22579	35.84282
	60	31.87474	35.06613	36.33818	36.97469
5000	0	41.76444	45.93988	47.60946	48.44675
	30	39.67622	43.64289	45.22899	46.02441
	60	40.92915	45.02109	46.65727	47.47781
6000	0	50.69103	55.75914	57.78878	58.8016
	30	48.15648	52.97118	54.89934	55.86152
	60	49.67721	54.64395	56.633	57.62557
7000	0	55.48214	61.02835	63.25064	64.35928
	30	52.70803	57.97694	60.08811	61.14132
	60	54.3725	59.80779	61.98563	63.0721
8000	0	65.36175	71.89813	74.5094	75.81963
	30	62.09366	68.30322	70.78393	72.02865
	60	64.05452	70.46016	73.01921	74.30324

Table 4: Resistance coefficients in laminar condition

f	α	$\omega = 0\%$	$\omega = 0.1\%$	$\omega = 0.3\%$	$\omega = 0.5\%$
800	0	0.07614	0.0769	0.07767	0.07844
	30	0.07738	0.07805	0.07883	0.07962
	60	0.07421	0.07536	0.07611	0.07687
1200	0	0.06428	0.06482	0.06547	0.06623
	30	0.065	0.06565	0.06631	0.06728
	60	0.0627	0.06353	0.06426	0.0649
1600	0	0.05678	0.05735	0.05792	0.0585
	30	0.05698	0.05806	0.05834	0.05902
	60	0.05564	0.0561	0.05686	0.05733
2000	0	0.05213	0.05265	0.05318	0.05371
	30	0.05243	0.05306	0.05359	0.05412
	60	0.05109	0.0516	0.05212	0.05264
2200	0	0.05196	0.05248	0.053	0.05353
	30	0.05216	0.05268	0.05321	0.05374
	60	0.05012	0.05143	0.05204	0.05246

Table 5: Resistance coefficients in turbulent condition

f	α	$\omega = 0\%$	$\omega = 0.1\%$	$\omega = 0.3\%$	$\omega = 0.5\%$
3000	0	0.04548	0.04594	0.0464	0.04686
	30	0.04567	0.04613	0.04659	0.04705
	60	0.04458	0.04502	0.04547	0.04593
4000	0	0.04367	0.04411	0.04455	0.04499
	30	0.04385	0.04429	0.04473	0.04518
	60	0.0428	0.04323	0.04366	0.04409
5000	0	0.04102	0.04143	0.04184	0.04226
	30	0.0412	0.04161	0.04203	0.04245
	60	0.0402	0.0406	0.04101	0.04142
6000	0	0.03717	0.03754	0.03791	0.03829
	30	0.03744	0.03781	0.03819	0.03857
	60	0.03684	0.03731	0.03758	0.03796
7000	0	0.03552	0.03587	0.03623	0.0367
	30	0.03609	0.03625	0.03681	0.03708
	60	0.03497	0.03532	0.03568	0.03603
8000	0	0.0338	0.03413	0.03448	0.03482
	30	0.03396	0.0343	0.03464	0.03499
	60	0.03313	0.03347	0.0338	0.03414

3.4 Comprehensive Evaluation

From above analysis, high nanoparticle and a rotation angle α = 0° not only increase the thermal performance but also increase the flow resistance, to scientifically evaluate them, a comprehensive evaluation performance index is introduced. The comprehensive index can be calculated by Eq. (13), and the corresponding results are given in Fig. 11. Fig. 11 illustrates that the Reynolds number has a significant impact on the comprehensive evaluation performance index, and the nanoparticle mass fraction has the same effect. The triangle tube with α = 0° shows the biggest comprehensive index, followed by the triangle tube with α = 60°, and the triangle tube with α = 30° is the minimal one. Nanofluids with ω = 0.5% in the triangle tube with α = 0° perform the biggest comprehensive evaluation performance index and it can reach 1.26, thus demonstrating that the influence of nanoparticles and Reynolds number on the ratio of enhancing heat exchange is bigger than that on the flow resistance.

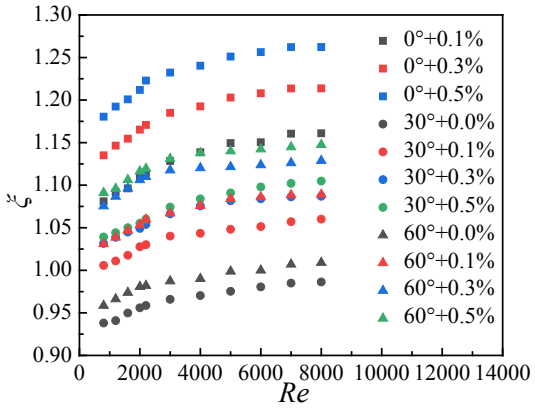

Figure 11: Comprehensive evaluation performance

4 Conclusions

The forced convection of TiO_2 nanofluids is experimentally discussed in a triangular tube at various rotation angles. The main results are as below:

(1) The triangular tube with a rotation angle α = 0° reveals the maximal Nusselt number, followed by the triangular tube with a rotation angle α = 60°, and the triangular tube with a rotation angle α = 30° has the lowest Nusselt number. A comparison between triangular tubes with rotation angles α = 0° and 30° illustrates that the maximum ratios on enhancing heat transfer are 6.2% and 5.3% for laminar and turbulent conditions respectively. The reason is that the triangle tube with a rotation angle α = 0° has the greatest impact on the reduction in laminar boundary layer.

(2) Resistance coefficients of the triangular tubes are close to each other, especially the rotation angles α = 0° and 30°, and the triangular tube with a rotation angle α = 60° behaves the minimal resistance coefficient. Compared with a rotation angle α = 60°, the maximal increments of resistance coefficient are 4.1% and 3.2% in the triangular tube with a rotation angle 30° for laminar and turbulent conditions respectively. This demonstrates that the resistance coefficients relate to the rotation angles directly as well.

(3) Nusselt number behaves an increment with the enlarged nanoparticle mass fraction. Compared with pure water, the maximal increments of the Nusselt number are 20.3% and 16% for nanofluids (ω = 0.5%) at laminar and turbulent conditions respectively. It is because the whole thermal conductivity of fluid can be increased after adding the TiO_2 nanoparticles. Besides, nanoscale nanoparticles have the greatest Brownian force compared with other interaction forces, which can augment the heat exchange performance.

(4) Addition of nanoparticles increases the resistance coefficient. Compared with pure water, the maximal increments of the resistance coefficient are 4.7% and 3.3% for nanofluids (ω = 0.5%) at laminar

and turbulent conditions respectively. The reason is that the drag force between water molecules and nanoparticles can increase the viscosity.

(5) The Reynolds number has a significant impact on the comprehensive evaluation performance index, and the nanoparticle mass fraction has the same effect. The triangle tube with $\alpha = 0°$ shows the biggest comprehensive index, followed by the triangle tube with $\alpha = 60°$, and the triangle tube with $\alpha = 30°$ has the smallest one.

Funding Statement: This work is financially supported by "Natural Science Foundation of Jiangsu Province, China" (Grant No. BK20181359).

Conflicts of Interest: The authors declare that they have no conflicts of interest to report regarding the present study.

References

1. Esfe, M. H., Esfandeh, S., Amiri, M. K., Afrand, M. (2019). A novel applicable experimental study on the thermal behavior of SWCNTs (60%)-MgO (40%)/EG hybrid nanofluid by focusing on the thermal conductivity. *Powder Technology, 342,* 998–1007.
2. Akhgar, A., Toghraie, D., Sina, N., Afrand, M. (2019). Developing dissimilar artificial neural networks (ANNs) to prediction the thermal conductivity of MWCNT-TiO_2/Water-ethylene glycol hybrid nanofluid. *Powder Technology, 355,* 602–610.
3. Wang, X., Yan, X., Gao, N., Chen, G. (2019). Prediction of thermal conductivity of various nanofluids with ethylene glycol using artificial neural network. *Journal of Thermal Science*.
4. Hu, Y., He, Y., Zhang, Z., Wen, D. (2017). Effect of Al_2O_3 nanoparticle dispersion on the specific heat capacity of a eutectic binary nitrate salt for solar power applications. *Energy Conversion and Management, 142,* 366–373.
5. Chen, M., He, Y., Wang, X., Hu, Y. (2018). Complementary enhanced solar thermal conversion performance of core-shell nanoparticles. *Applied Energy, 211,* 735–742.
6. Hu, Y., Li, H., He, Y., Liu, Z., Zhao, Y. (2017). Effect of nanoparticle size and concentration on boiling performance of SiO_2 nanofluid. *International Journal of Heat and Mass Transfer, 107,* 820–828.
7. Salimpour, M. R., Abdollahi, A., Afrand, M. (2017). An experimental study on deposited surfaces due to nanofluid pool boiling: comparison between rough and smooth surfaces. *Experimental Thermal and Fluid Science, 88,* 288–300.
8. Li, Z., Sheikholeslami, M., Chamkha, A. J., Raizah, Z. A., Saleem, S. (2018). Control volume finite element method for nanofluid MHD natural convective flow inside a sinusoidal annulus under the impact of thermal radiation. *Computer Methods in Applied Mechanics and Engineering, 338,* 618–633.
9. Izadi, M., Sinaei, S., Mehryan, S. A. M., Oztop, H. F., Abu-Hamdeh, N. (2018). Natural convection of a nanofluid between two eccentric cylinders saturated by porous material: buongiorno's two phase model. *International Journal of Heat and Mass Transfer, 127,* 67–75.
10. Izadi, M., Mohebbi, R., Chamkha, A., Pop, I. (2018). Effects of cavity and heat source aspect ratios on natural convection of a nanofluid in a C-shaped cavity using lattice Boltzmann method. *International Journal of Numerical Methods for Heat & Fluid Flow, 28(8),* 1930–1955.
11. Zhao, N., Guo, L., Qi, C., Chen, T., Cui, X. (2019). Experimental study on thermo-hydraulic performance of nanofluids in CPU heat sink with rectangular grooves and cylindrical bugles based on exergy efficiency. *Energy Conversion and Management, 181,* 235–246.
12. Sheikholeslami, M., Keramati, H., Shafee, A., Li, Z., Alawad, O. A. et al. (2019). Nanofluid MHD forced convection heat transfer around the elliptic obstacle inside a permeable lid drive 3D enclosure considering lattice Boltzmann method. *Physica A: Statistical Mechanics and Its Applications, 523,* 87–104.
13. Sheikholeslami, M., Farshad, S. A., Shafee, A., Tlili, I. (2019). Modeling of solar system with helical swirl flow device considering nanofluid turbulent forced convection. *Physica A: Statistical Mechanics and Its Applications*.

14. Karimipour, A., Taghipour, A., Malvandi, A. (2016). Developing the laminar MHD forced convection flow of water/FMWNT carbon nanotubes in a microchannel imposed the uniform heat flux. *Journal of Magnetism and Magnetic Materials, 419,* 420–428.
15. Karimipour, A., Nezhad, A. H., D'Orazio, A., Esfe, M. H., Safaei, M. R. et al. (2015). Simulation of copper-water nanofluid in a microchannel in slip flow regime using the lattice Boltzmann method. *European Journal of Mechanics-B/Fluids, 49,* 89–99.
16. Sun, B., Guo, Y., Yang, D., Li, H. (2020). The effect of constant magnetic field on convective heat transfer of Fe_3O_4/water magnetic nanofluid in horizontal circular tubes. *Applied Thermal Engineering, 171,* 114920.
17. Sun, B., Zhang, Y., Yang, D., Li, H. (2019). Experimental study on heat transfer characteristics of hybrid nanofluid impinging jets. *Applied Thermal Engineering, 151,* 556–566.
18. Mei, S., Qi, C., Liu, M., Fan, F., Liang, L. (2019). Effects of paralleled magnetic field on thermo-hydraulic performances of Fe_3O_4-water nanofluids in a circular tube. *International Journal of Heat and Mass Transfer, 134,* 707–721.
19. Li, Z., Sheikholeslami, M., Jafaryar, M., Shafee, A., Chamkha, A. J. (2018). Investigation of nanofluid entropy generation in a heat exchanger with helical twisted tapes. *Journal of Molecular Liquids, 266,* 797–805.
20. Pak, B. C., Cho, Y. I. (1998). Hydrodynamic and heat transfer study of dispersed fluids with submicron metallic oxide particles. *Experimental Heat Transfer, 11(2),* 151–170.
21. Qi, C., Wan, Y. L., Li, C. Y., Han, D. T., Rao, Z. H. (2017). Experimental and numerical research on the flow and heat transfer characteristics of TiO_2-water nanofluids in a corrugated tube. *International Journal of Heat and Mass Transfer, 115(Part B),* 1072–1084.
22. Sieder, E. N., Tate, G. E. (1936). Heat transfer and pressure drop of liquids in tubes. *Industrial & Engineering Chemistry, 28,* 1429–1435.
23. Nieolinski, V. (1976). New equations for heat mass transfer in turbulent pipe and channel flows. *International Chemical Engineering, 16,* 359–368.
24. Yang, S. M., Tao, W. Q. (2006). *Heat transfer*. Higher Education Press, China.
25. Qi, C., Wang, G., Yang, L., Wan, Y., Rao, Z. (2017). Two-phase lattice Boltzmann simulation of the effects of base fluid and nanoparticle size on natural convection heat transfer of nanofluid. *International Journal of Heat and Mass Transfer, 105,* 664–672.